

GPU-based track-finding for the J-PARC muon g-2/EDM experiment

Hridey Chetri^{1a} **Deepak Samuel**^{2b} **Saurabh Sandilya**^a **Takashi Yamanaka**^c **Tsutomu Mibe**^d **Taikan Suehara**^e

^a*Indian Institute of Technology Hyderabad,
Hyderabad, India*

^b*Central University of Karnataka,
Karnataka, India*

^c*Kyushu University,
Fukuoka, Japan*

^d*Institute of Particle and Nuclear Studies (IPNS),
KEK, Japan*

^e*ICEPP, University of Tokyo,
Tokyo, Japan*

E-mail: deepaksamuel@cuk.ac.in

ABSTRACT: The muon $g-2$ /EDM experiment at J-PARC is designed to precisely measure the muon's magnetic moment and electric dipole moment, driven by discrepancies between theory and previous experiments. A key challenge is the fast reconstruction of positron tracks from multiple muon decays within a short time span causing an event pileup. One of the aspects is the identification of individual positron tracks from the reconstructed hits, which is currently done using a hough-transform based approach. Results from simulation studies have shown expected results in terms of efficiency and accuracy of track reconstruction. However, the execution time for the entire analysis chain is prohibitively long to be deployed in the experiment. Specifically, preliminary estimations suggest a requirement of $40 \times$ speedup of the track-finding routine. In this context, we explore a GPU-based solution to accelerate track-finding through parallel processing and present the implementation details and the results of our study for different pileup conditions. The results indicate that the GPU solution far exceeds our expectation in terms of execution speed without compromising on the reconstruction efficiency.

KEYWORDS: Hough Space, GPU computing, Pattern recognition, cluster finding, CUDA, Kernel, shared memory

¹First author.

²Corresponding author.

Contents

1	Introduction	1
2	Experimental Method	2
3	Simulation studies	3
4	Track Finding	5
5	CPU Based Approach	5
6	GPU based approach	6
7	Analysis	8
8	Summary and conclusion	11

1 Introduction

The most recent measurement of the muon’s magnetic anomaly, a_μ , by the Fermilab Muon $g-2$ experiment, using data from Runs 1 through 6, has achieved a remarkable precision of 127 parts per billion (ppb) [1]. This measurement provides a stringent test of the Standard Model [2, 3]. Complementary to the Fermilab experiment, the J-PARC muon $g-2$ /EDM experiment aims to measure both a_μ and η . They are defined by the relations

$$a_\mu = \frac{g - 2}{2}, \quad \vec{\mu}_\mu = g \left(\frac{e}{2m} \right) \vec{s}, \quad \vec{d}_\mu = \eta \left(\frac{e}{2mc} \right) \vec{s}, \quad (1.1)$$

where e , m , and \vec{s} are the electric charge, mass, and spin vector of the muon, respectively. Here, g is the Landé g -factor and η is a corresponding factor for the EDM [4, 5]. It is determined by precisely measuring the spin precession frequency of muons stored in a magnetic field [6]. The muon $g-2$ /EDM experiment aims to measure a_μ and η with high precision using ultraslow muons, providing an independent avenue to search for potential signs of new physics beyond the Standard Model and to cross-validate the Fermilab result with an independent measurement using a new technique [7–10]. The SM prediction of a_μ^{SM} from the 2020 white paper [11] and the experimental value of a_μ^{exp} from the 2023 Fermilab result [12] are as follows, respectively:

$$a_\mu^{\text{SM}} = 116\,591\,810(43) \times 10^{-11}, \quad a_\mu^{\text{exp}} = 116\,592\,059(22) \times 10^{-11}, \quad (1.2)$$

where the uncertainties are from the electroweak, leading-order hadronic, and higher-order hadronic contributions in a_μ^{SM} . The errors are the statistical, systematic, and external parameter uncertainties combined in quadrature in a_μ^{exp} . A comparison between the Fermilab result from Run-1/2/3

presented here, $a_\mu(\text{exp})$, and the prediction from the 2020 white paper yields a discrepancy of 5.0σ . This deviation from the SM prediction could hint at new physics, motivating more precise measurements of a_μ .

The result from the current experimental measurement[1, 10, 13], and the updated prediction of a_μ from white paper 2025 [13, 14] is given by:

$$\Delta a_\mu \equiv a_\mu^{\text{exp}} - a_\mu^{\text{SM}} = 116592071.5(14.5) \times 10^{-11} - 116592033(62) \times 10^{-11} = 38(63) \times 10^{-11} \quad (1.3)$$

Though the new results have reduced the tension between the SM model value and experimental value of a_μ , it is important and intriguing to validate the experimental result with a new approach and new systematics. The J-PARC muon g -2/EDM experiment is designed to measure a_μ and η using a technique different from that used in previous experiments that used the magic gamma approach [10].

In this note, we explore the use of GPU parallelism [15] to speed up the track-finding process, using Geant4[16]-simulated positron tracks generated with the "g2esoft" framework, which is developed for simulation and track reconstruction for the J-PARC muon g -2/EDM experiment. Section 2 briefly describes the experimental setup of the J-PARC muon g -2/EDM experiment. Simulation studies follow this in Section 3, the track-finding procedure in Section 4, and a comparison between CPU- and GPU-based approaches in Sections 5 and 6, respectively. Finally, we analyze the performance results in Section 7 and present our conclusions in Section 8.

2 Experimental Method

A primary 3 GeV proton beam from the J-PARC accelerator strikes a graphite target to produce secondary particles, including muons [17]. Surface muons which can reach a maximum momentum of 29.8 MeV/c are extracted through the H-line beamline [18]. At a proton beam power of 1 MW, the expected muon beam intensity reaches approximately 10^8 muons per second. These surface muons are injected into a room-temperature silica aerogel target, where they are slowed down, thermalized, and form muonium (Mu) atom [19, 20]. The thermalized Mu atoms diffuse into an adjacent vacuum region, where they are ionized by laser irradiation to generate ultraslow muons [21]. The resulting muons are reaccelerated to a momentum of 300 MeV/c with 50% polarization and vertically injected into a compact storage ring [22, 23]. This ring employs an MRI-type solenoid magnet that provides a highly uniform magnetic field of 3 T, with a precision of 1 ppm within the 66 cm diameter storage region [24, 25]. A novel vertical injection scheme significantly improves injection efficiency by more than an order of magnitude. The ring uses weak magnetic focusing to maintain the muon orbit, and silicon-strip detectors [26] are placed inside the field to track the decay positrons and measure their momenta. The detector aims to measure the muon's anomalous spin precession frequency, ω_a , and the up-down asymmetry of positron emission caused by the electric dipole moment (EDM). After acceleration to 300 MeV/c, the muon beam arrives in 10 ns-wide pulses consisting of three microbunches, with a repetition rate of 25 Hz. Each pulse, or "fill," injects about 10^4 muons into the storage ring. Shortly after each fill, approximately 30 positrons from muon decays are detected within a 5 ns time window [7]. Figure 1 shows the schematic diagram of the muon g -2/EDM experimental setup with graphite target, LINAC, and positron detector(lateral view and top view). The detector consists of 40 radial modules called vanes. Each vane consists of 16 sensors, half of

which measure the radial coordinate and half the axial coordinate of ionization. To ensure good acceptance, the sensitive area along the axial direction is set to ± 200 mm. For efficient detection of mid momentum positrons ($200 \text{ MeV}/c < p < 275 \text{ MeV}/c$), the radial sensitive range is from $r = 70$ mm to $r = 290$ mm. The active area of each sensor is $97.28 \text{ mm} \times 97.28 \text{ mm}$ with a thickness of 0.32 mm. A sensor contains two blocks of 512 strips with a pitch of $190 \mu\text{m}$. Therefore, a vane has 16,384 strips, and the detector has a total of 655k strips.

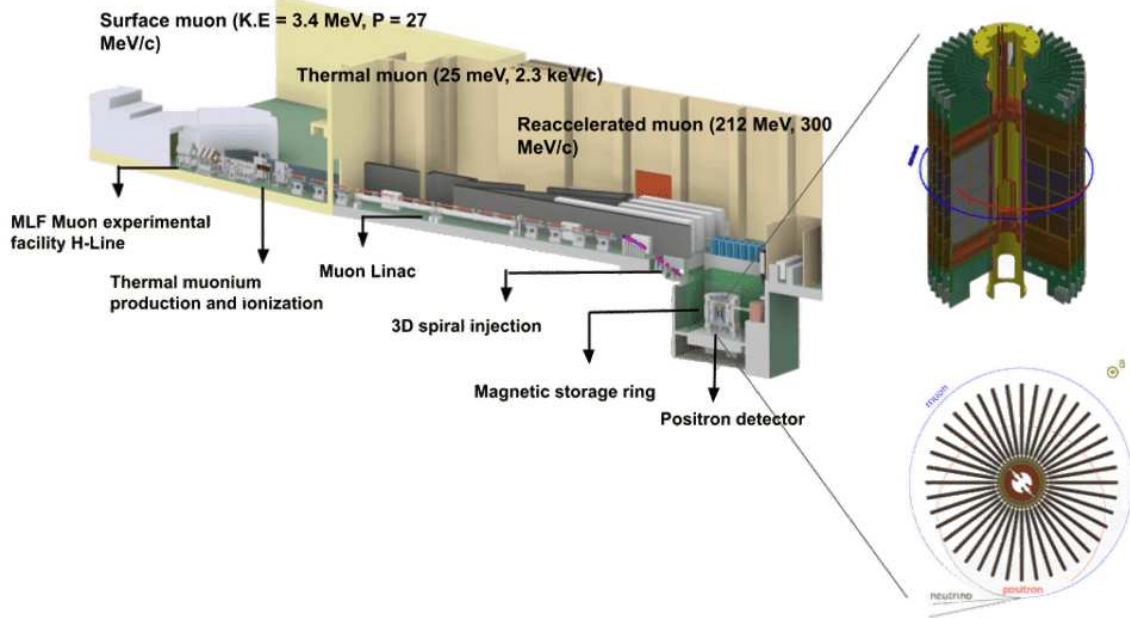


Figure 1: Schematic view of the muon $g - 2$ /EDM experiment at J-PARC MLF

3 Simulation studies

In order to benchmark the performance of algorithms, a simulation framework for J-PARC muon $g - 2$ /EDM experiment has been developed. The standard simulation workflow is illustrated in Figure 2. The detector simulation stage uses the Geant4 toolkit to model muon decay and the interactions of decay positrons with detector materials. By default, each event simulates a single muon decay. An ideal $300 \text{ MeV}/c$ muon beam circulates at a radial position of $r \sim 333$ mm and vertical position $z = 0$, within a uniform 3 T magnetic field oriented along the z -axis. Standard electromagnetic processes are used to model interactions of charged particles with matter, and energy loss due to synchrotron radiation is also included for positrons and electrons.

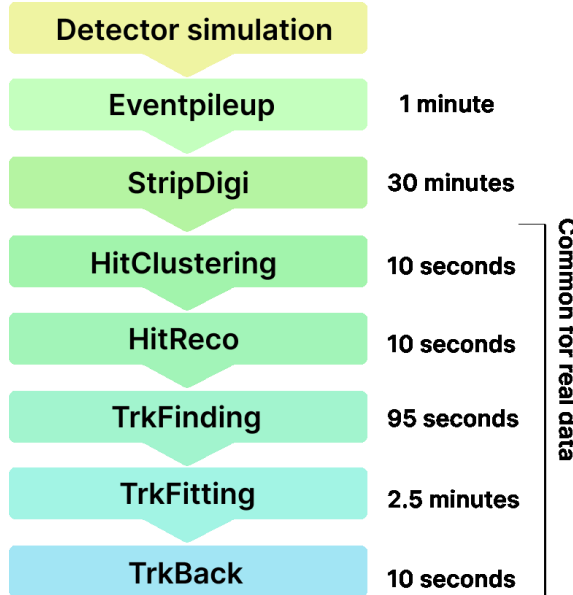


Figure 2: Standard processing order of simulation, digitization and track reconstruction (Computation time required for each process is mentioned towards right).

The next step in simulation is, EventPileup, merges multiple events simulated at the detector simulation stage into a single event to emulate the pile-up of muon decay events. The "StripDigi" module performs digitization by converting simulated hits (SimHits) into strip-level hits (StripHits), accurately reconstructing their spatial and temporal information to reflect the detector resolution and response characteristics. The "HitClustering" processor generates "StripClusters" by merging adjacent StripHits. HitReco creates RecoHits by combining StripClusters in R and Z sensors. These "RecoHits" are used as input for track finding, which is discussed in the subsequent section in a little more detail. Track reconstruction is performed by the "TrkFitting" module, which fits particle trajectories using input data from either "RecoHits" or "StripClusters". These inputs correspond to processed signals from the tracking detectors. The track parameters are estimated at the position of the first detector hit using the Kalman filter algorithm, as implemented in the Genfit2 toolkit [27]. Once the tracks have been reconstructed, the "TrackBack" module extrapolates them backward to the muon orbit in order to estimate the decay vertex. This step is essential for reconstructing the decay topology and associating tracks with their parent muons. The extrapolation is applied exclusively to tracks that are not identified as ghosts-false or ambiguous reconstructions typically arising from noise or misidentified hits. The positron track is extrapolated starting from the estimated position and momentum at the first detector hit. The muon orbit is modeled as a fixed circular trajectory in a plane perpendicular to the z -axis, consistent with the storage ring configuration. In contrast, the positron trajectory is approximated as a helix, arising from its motion in the uniform magnetic field along the z -direction. The muon decay position is then estimated as the point of closest approach between the muon and positron trajectories in three-dimensional space. This geometrical construction ensures accurate localization of decay vertices, which is critical for downstream analysis such as lifetime measurements and background suppression.

4 Track Finding

A general example of track finding for $g-2/EDM$ experiment is described in simple steps in Figure 3. Positrons from muon decays travel in a helical trajectory within the magnetic storage ring. When this trajectory is projected onto the ϕ - z plane, it appears as a straight line with a certain slope and intercept. To identify these lines, the Hough Transform algorithm [28, 29] is employed. This technique is particularly effective in detecting geometric shapes such as lines or circles even in data that is noisy, sparse, or has overlapping patterns. Each point in the ϕ - z plane can be transformed into a sinusoidal curve in the Hough space, defined by the parameters (ρ, θ) , through the relation [30]:

$$\rho = \phi \cos \theta + z \sin \theta. \quad (4.1)$$

In the Hough space, intersections of these curves represent potential straight lines formed by multiple hits in the ϕ - z plane. The bin with the highest accumulation in Hough space indicates the most probable line candidate. Once a line is identified in the ϕ - z plane, the corresponding RecoHits lying along it are used as seeds to reconstruct the full track in three-dimensional space.

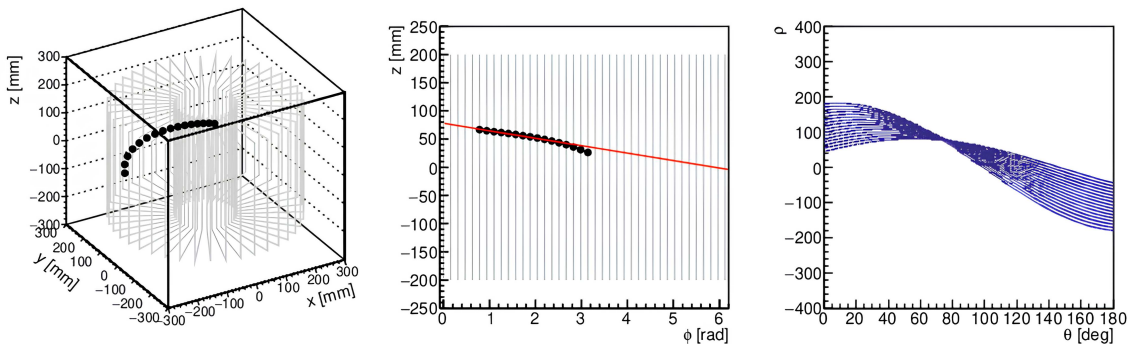


Figure 3: An example muon decay event. Left: RecoHits in three-dimensional space. Middle: projection onto the ϕ - z plane. Right: the corresponding Hough space. The most populated bin in Hough space corresponds to the red line in the ϕ - z plane.

Track extension is performed by selecting three RecoHits (Track seed) on consecutive vanes and extrapolating their trajectory to search for additional hits on neighboring vanes in the forward or backward direction. This search is confined within a fixed time window of width 10 ns. When no more RecoHits can be added within the current window, the window is shifted by a step size of 5 ns, and a new track-finding process begins. If the flag for finding the tracks in the next time window is set to true from the previous time window, then the algorithm first attempts to continue building the previously identified track candidates in the new time window before initiating a completely new search. This iterative procedure ensures efficient reconstruction of positron tracks even in high-occupancy or pile-up scenarios.

5 CPU Based Approach

Track finding on the CPU is performed sequentially through the following steps. First, the reconstructed hit points (reco-hits) are divided into overlapping time windows of 10 ns, with a sliding

step of 5 ns. Within each time window, the spatial coordinates (x, y, z) of the hits are transformed into the (ϕ, z) space, where $\phi = \tan^{-1}(y/x)$. The transformed (ϕ, z) points are then mapped to a Hough space using the Hough Transform equation (Eq. 4.1). This results in a 2D histogram with θ and ρ as axes. The histogram is binned into 180 bins in θ (ranging from 0° to 180°) and 1000 bins in ρ (ranging from -500 to 500). Each hit contributes to multiple bins based on its possible track parameters. After the histogram is filled, a peak-finding algorithm identifies the bin with the highest number of entries. The corresponding (θ, ρ) values are interpreted as the most probable track parameters in the (ϕ, z) plane. Using these peak values, track seeds are found by selecting the hits that align with the straight line formed by the identified (θ, ρ) . These seeds serve as the initial candidates for tracks. A track extrapolation step then follows, which refines the track by extending it across layers and associating additional hits based on geometric and timing consistency. This entire process—time slicing, coordinate transformation, Hough mapping, peak detection, seed finding, and track extrapolation—is repeated for each time window. While conceptually straightforward, this sequential CPU-based approach is computationally intensive, especially in sorting hits, populating the Hough histogram, and extrapolation.

Figure 2 shows the sequence of simulation steps along with the corresponding timestamps. Some of these steps are also used in real data processing. The most time-consuming parts are track finding and track fitting, which currently take approximately 95 seconds and 280 seconds, respectively for 10^4 muon decay. Currently, data acquisition operates at a rate of approximately 10^4 muons every 7 minutes, which corresponds to about 24 muons per second per CPU. With 1000 CPUs, the overall data processing rate reaches roughly 2.4×10^4 muons per second. However, the experiment is expected to record data from around 10^{13} muon decays in total. The beam intensity will be 4×10^4 muons per pulse at 25 Hz, yielding a rate of 10^6 muons per second. Therefore, to keep up with the data taking rate, the software must be capable of processing data from approximately 10^6 muon decays per second. This implies that the current software speed needs to improve by a factor of about 10 to meet the experimental requirements.

6 GPU based approach

Unlike CPUs, which have only a few powerful cores, GPUs have a much larger number of threads (cores) that can run at the same time. While each individual thread may be slower than a CPU core in terms of processing power, the massive parallelism allows GPUs to handle large-scale computations efficiently. In the J-PARC muon $g-2$ /EDM experiment, track finding involves processing a large number of detector hits to reconstruct particle trajectories. Traditionally, this process is performed in sequence on a CPU, starting from the Hough Transform, followed by helical track seed fitting, and then extrapolation. This sequential processing is computationally expensive due to the high volume of hit data.

To improve performance, we utilize a GPU-based approach, where detector hits are processed in parallel. In this method, each detector hit is mapped to a GPU thread, and a certain number of threads form a block. All threads within a block work together to fill a histogram in shared memory (as described in later in this Section), allowing efficient collection of votes during the Hough Transform step. Track seed finding, Helical track fitting, and extrapolation are also performed in parallel across threads for each block. To organize the processing, hits are divided into 10 ns time

windows, with each GPU block handling one time window. Within each block, all steps—from Hough Transform to track fitting—are carried out simultaneously, significantly speeding up the reconstruction. For example, assuming processing of one time window on the CPU takes t seconds. Then, processing 100 such windows sequentially would take; $\sim 100 \times t$ seconds. While individual GPU threads are slower than CPU cores, they operate concurrently. If processing one time window on the GPU takes $10 \times t$ seconds due to thread overheads, all 100 windows can still be processed simultaneously in; $\sim 10 \times t$ seconds. Thus, the GPU-based approach, by leveraging massive parallelism, achieves a significant speed-up in track reconstruction despite slower individual cores. As shown in Figure 2 and discussed in the previous section, the total time required to process one event(10^4 muon tracks) of experimental data is approximately 420 seconds. The most time-consuming steps are track finding and track fitting. To achieve our goal of reducing the processing time to around 40 seconds, the overall computation time must be improved by a factor of 10, as noted in Section 5. All the steps mentioned in Section 5 are done in sequence on the CPU which make them computationally expensive. At this point GPU can be a suitable alternative to achieve acceleration in the track finding process. A GPU (Graphics Processing Unit) is a processor designed to handle many calculations at the same time using thousands of parallel cores. In track finding, the GPU speeds up the process by performing the coordinate transformation, Hough mapping, and track reconstruction in parallel.

GPU memory differs from CPU memory in both structure and access patterns [31]. As shown in Figure 4, each GPU block has its own *shared memory*, which is accessible by all threads within that block. In addition to shared memory, GPUs also include several other types of memory, each designed for specific use cases.

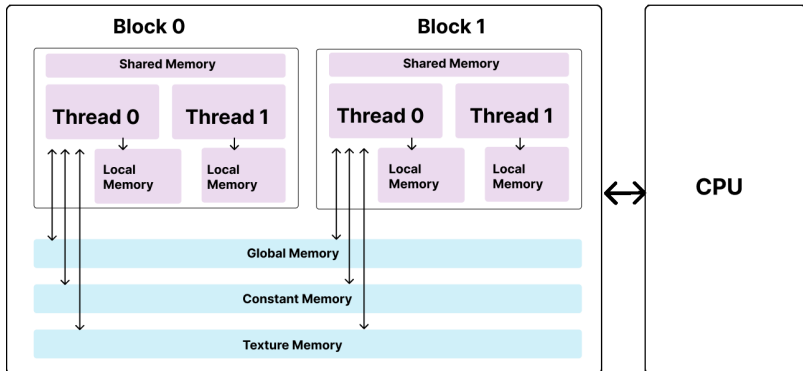


Figure 4: Schematic overview of the GPU memory distribution and its components [31].

However, the amount of shared memory available per block is limited. This poses challenges when constructing large data structures like the Hough space. To overcome this, we perform the Hough transformation into two stages: a coarse-binning histogram followed by a fine-binning histogram. This approach allows us to meet the binning requirements specified in the experiment while staying within the GPU's shared memory constraints, as illustrated in Figure 5.

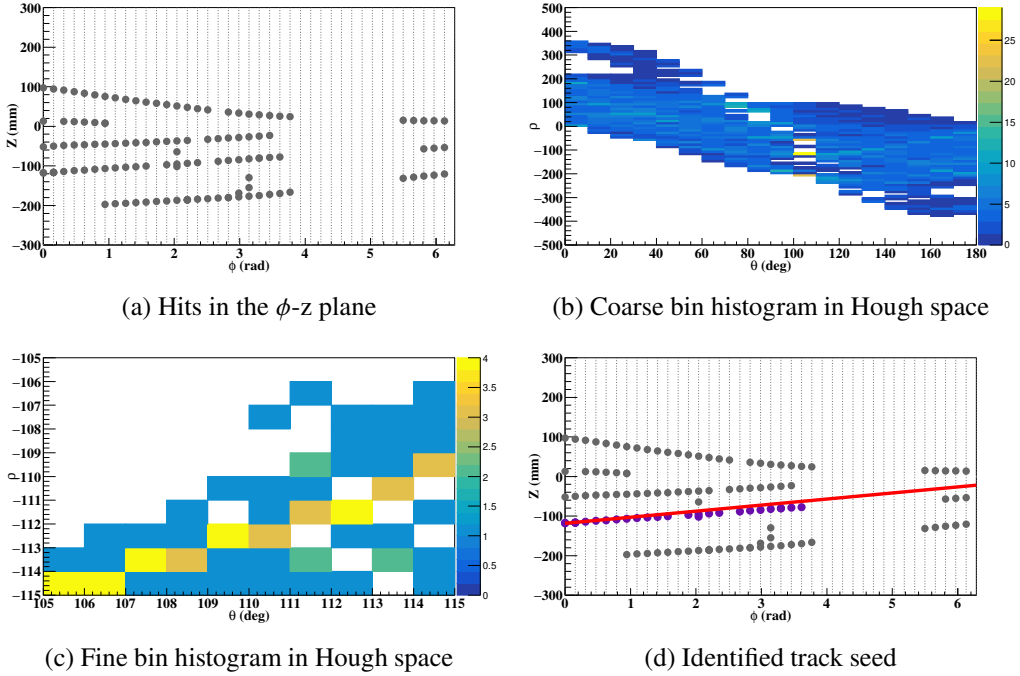


Figure 5: Steps in the Hough Transform for track seed identification, showing hits in the ϕ - z plane, Hough space histograms, and the final seed.

7 Analysis

Using the simulator and the track finding tool, the track finding efficiency in a multiple-track condition is estimated. The efficiency, ε , is defined as follows:

$$\varepsilon = \frac{N_{\text{found}}}{N_{\text{all}}}, \quad (7.1)$$

where N_{found} and N_{all} are the numbers of found tracks and all tracks, respectively. A track is regarded as found if its hits are reconstructed and clustered in continuous five vanes of the detector. We note that tracks with momentum greater than 200 MeV/ c have a sufficient number of hit points in the silicon vanes.

The generated momentum distribution and the reconstructed momentum distribution for different pileup rates of the positron tracks are shown in Figure 6 respectively.

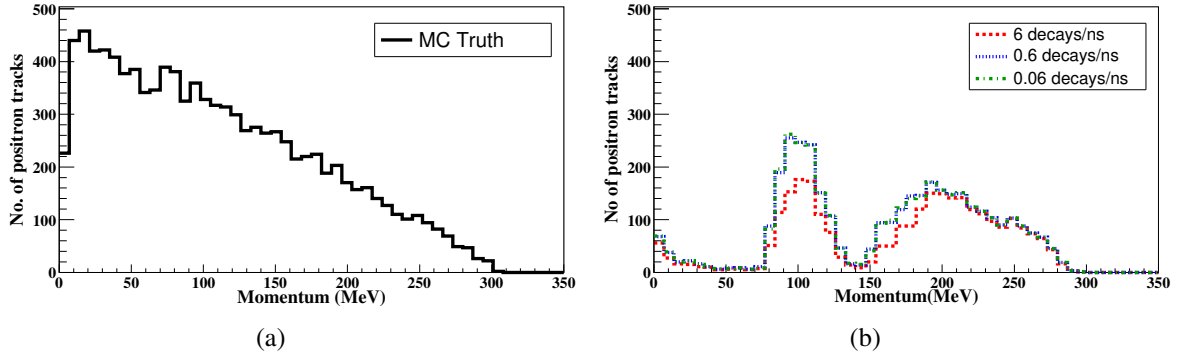


Figure 6: (a) Generated momentum distribution (b) Momentum distribution of found positron tracks

Figure 7 shows the track-finding efficiency for a single track as a function of the positron momentum under different track rate conditions. Even under the highest track rate condition of 6 tracks/ns, the finding efficiency remains above 90% in the momentum range of $200 \text{ MeV}/c < p < 275 \text{ MeV}/c$.

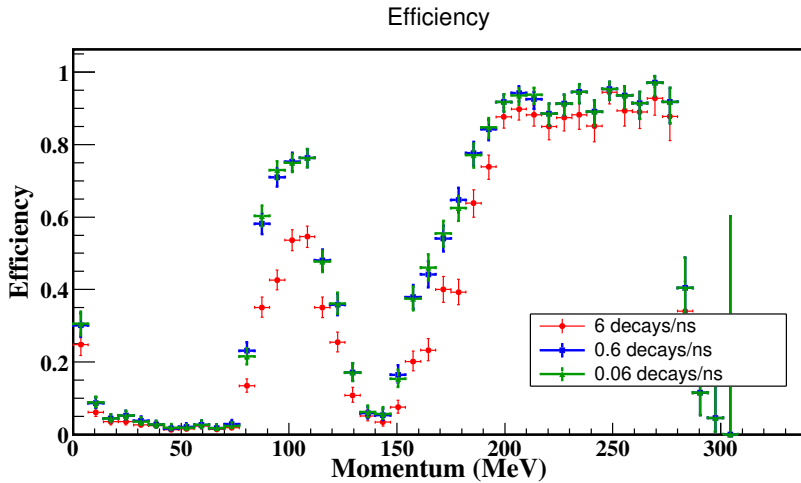


Figure 7: Momentum dependence of track finding efficiency with different conditions of track rates from 0.06 tracks/ns to 6 tracks/ns.

Tracking detectors can occasionally reconstruct false hits and tracks, known as ghost hits and ghost tracks. To evaluate their impact, the contribution of ghost hits in reconstructed tracks is studied for single-track events. It is found that approximately 50% of the tracks are found without any ghost hits, and the majority of the remaining tracks contain less than 20% ghost hit contribution. Some of the contributions from ghost hits are removed during the track-fitting process, and with a more optimized track-finding algorithm, they can be further reduced.

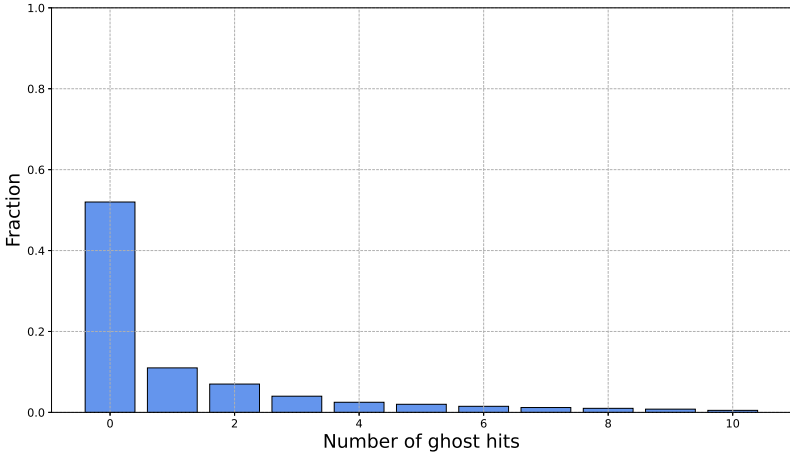


Figure 8: The fraction of ghost hits in the found tracks.

The computation times for GPU activities, including kernel execution and data transfers between host and device (both Host-to-Device and Device-to-Host), are summarized in Table 1. These measurements were obtained using the `nvprof` profiling tool for track rates ranging from 0.06 to 6 tracks/ns on a Tesla P100-PCIE GPU with 16 GiB of memory, using 10^4 simulated muon decay events.

		0.06 μ decay/ns	0.6 μ decay/ns	6.0 μ decay/ns
GPU based	GPU Kernel	17.00 s	58.00 s	118.00 s
	Memcpy HtD	70.00 ms	70.00 ms	60.00 ms
	Memcpy DtH	90.00 ms	90.00 ms	80.00 ms
CPU based	CPU (AMD7)	119 s	240 s	345 s

Table 1: Approximate Computation time for GPU kernel execution, CPU, and memory transfers at varying muon decay rates of 10^4 muons, measured using `nvprof` [32].

The computation time on GPUs depends on several key factors. These include the memory bandwidth, compute capability, number of processing cores, and clock speed. Other important factors are the amount of shared memory, register size, and how efficiently the algorithm uses memory. In addition, performance is influenced by the number of threads that can run in parallel (occupancy), the overhead of launching GPU kernels, and the time taken to transfer data between the CPU and GPU. Table 2 compares different GPUs based on important features like architecture, bandwidth, CUDA cores, and performance. A comparison is done on performance between different GPUs currently available in the market with 10^4 muons decaying at the rate of 0.06 muons/ns. Figure 9 shows the performance comparison between different GPUs.

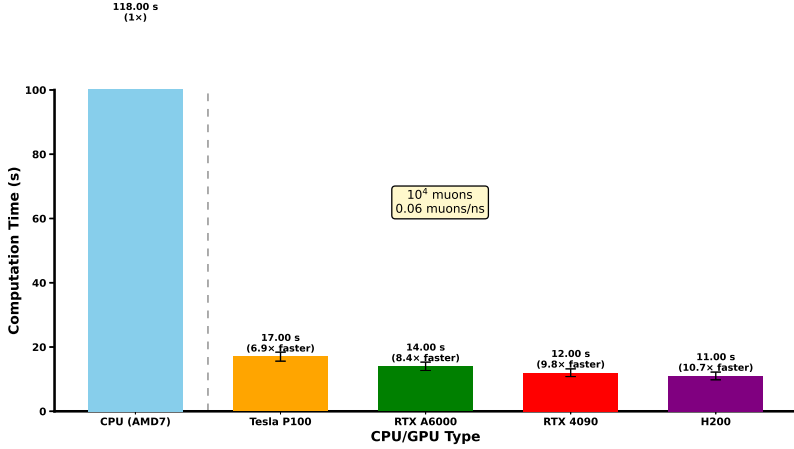


Figure 9: Approximated GPU performance comparison with different GPU architectures for 0.06 muon decays/ns

Spec / GPU	Tesla P100	RTX A6000	RTX 4090	NVIDIA H200
Architecture	Pascal	Ampere	Ada Lovelace	Hopper
FP32 TFLOPS	10.6	38.7	82.6	~60
Tensor TFLOPS	21.2	312	~330	2,000+
Memory Size	16 GB HBM2	48 GB GDDR6	24 GB GDDR6X	141 GB HBM3e
Bandwidth	732 GB/s	768 GB/s	1,008 GB/s	~4,800 GB/s
CUDA Cores	3,584	10,752	16,384	132 SMs + Tensor Cores

Table 2: Architecture comparison of Tesla P100, RTX A6000, RTX 4090, and NVIDIA H200 GPUs [33–36]

8 Summary and conclusion

Muon $g-2$ /EDM experiment at J-PARC measures the a_μ and EDM with a new approach to reach the uncertainty of 460 ppb. One of the crucial part of the analysis lies in the reconstruction of the positron tracks. These positron tracks are reconstructed from the hits in silicon strip detector. In the experiment, data collection (acquisition) can run the expected speed of 10^4 muons every 7 minutes(24 muons/sec/CPU). With 1000 CPUs, the data processing rate reaches about 10^5 muons per second. The software must handle data from approximately 10^6 muon decays per second (see Section 5).

With the implementation of the GPU for specification algorithm in track finding, we are able to accelerate the computation time by a factor of around $7 \times$ for the pileup rate of 0.06 muon decay/ns. (see Table 1). The efficiency is for the three pileup rate (0.06 tracks/ns, 0.6 tracks/ns and, 6 tracks/ns) is 90 - 95 %. We evaluated the ghost hit contamination at the lowest pile-up rate. As shown in Fig. 8, approximately 50% of the tracks are reconstructed without any ghost hits.

Among the remaining tracks, the majority exhibit a ghost hit contribution of less than 20%. As discussed in Section 7, Figure 9 shows that GPU-based processing significantly speeds up the track finding process. This improvement is attributed to the GPU’s higher compute capability, greater memory bandwidth, and large number of parallel processing cores, offering a clear advantage over traditional CPU-based methods. In particular, the NVIDIA RTX 4090 and H200 achieves over a tenfold improvement in performance compared to CPU-based methods.

In the simulation framework, track fitting is one of the most time-consuming steps. It uses input from either `RecoHits` or `StripClusters`, which are processed signals from the tracking detectors. The track parameters are estimated at the position of the first detector hit using the Kalman filter algorithm, as implemented in the Genfit2 toolkit [27]. To further speed up the simulation, the next step in our study could be to implement the track fitting algorithm on the GPU. By rewriting both the track finding and track fitting algorithms to run entirely on the GPU, we can significantly accelerate the overall simulation process.

Acknowledgements

This work was supported in part by JSPS Kakenhi Grants No. 20H05625 and 22K21350.

References

- [1] T.M. *g*–2 Collaboration, :, D.P. Aguillard, T. Albahri, D. Allspach, J. Annala et al., *Measurement of the positive muon anomalous magnetic moment to 127 ppb*, 2025.
- [2] S. Weinberg, *A model of leptons*, *Phys. Rev. Lett.* **19** (1967) 1264.
- [3] G. Altarelli and S. Forte, *The Standard Model of Electroweak Interactions*, in *Particle Physics Reference Library. Volume 1: Theory and Experiments*, H. Schopper, ed., pp. 35–81 (2020), DOI.
- [4] A. Keshavarzi, D. Nomura and T. Teubner, *Muon $g - 2$ and $\alpha(M_Z^2)$: A new data-based analysis*, *Phys. Rev. D* **97** (2018) 114025.
- [5] F. Jegerlehner, *The Anomalous Magnetic Moment of the Muon*, vol. 274, Springer, Cham (2017), 10.1007/978-3-319-63577-4.
- [6] L. Thomas, *I. the kinematics of an electron with an axis*, *The London, Edinburgh, and Dublin Philosophical Magazine and Journal of Science* **3** (1927) 1 [<https://doi.org/10.1080/14786440108564170>].
- [7] M. Abe, S. Bae, G. Beer, G. Bunce, H. Choi, S. Choi et al., *A new approach for measuring the muon anomalous magnetic moment and electric dipole moment*, *Progress of Theoretical and Experimental Physics* **2019** (2019) 053C02 [<https://academic.oup.com/ptep/article-pdf/2019/5/053C02/28746337/ptz030.pdf>].
- [8] J. Grange, V. Guarino, P. Winter, K. Wood, H. Zhao, R. Carey et al., *Muon (g-2) technical design report*, .
- [9] A. Keshavarzi, K.S. Khaw and T. Yoshioka, *Muon g –2: A review*, *Nuclear Physics B* **975** (2022) 115675.
- [10] MUON g-2 COLLABORATION collaboration, *Final report of the e821 muon anomalous magnetic moment measurement at bnl*, *Phys. Rev. D* **73** (2006) 072003.

- [11] T. Aoyama, N. Asmussen, M. Benayoun, J. Bijnens, T. Blum, M. Bruno et al., *The anomalous magnetic moment of the muon in the standard model*, *Physics Reports* **887** (2020) 1.
- [12] D. Aguillard, T. Albahri, D. Allspach, A. Anisenkov, K. Badgley, S. Baeßler et al., *Measurement of the positive muon anomalous magnetic moment to 0.20 ppm*, *Physical Review Letters* **131** (2023) .
- [13] PARTICLE DATA GROUP collaboration, *Review of particle physics*, *Phys. Rev. D* **98** (2018) 030001.
- [14] R. Aliberti, T. Aoyama, E. Balzani, A. Bashir, G. Benton, J. Bijnens et al., *The anomalous magnetic moment of the muon in the standard model: an update*, 2025.
- [15] J.D. Owens, M. Houston, D. Luebke, S. Green, J.E. Stone and J.C. Phillips, *Gpu computing*, *Proceedings of the IEEE* **96** (2008) 879.
- [16] S. Agostinelli, J. Allison, K. Amako, J. Apostolakis, H. Araujo, P. Arce et al., *GEANT4—A Simulation Toolkit*, *Nuclear Instruments and Methods in Physics Research Section A: Accelerators, Spectrometers, Detectors and Associated Equipment* **502** (2003) 250.
- [17] *Renovation of a scraper unit of a muon production target at j-parc*, in *Proceedings of the 14th International Conference on Muon Spin Rotation, Relaxation and Resonance (μ SR2017)* DOI [<https://journals.jps.jp/doi/pdf/10.7566/JPSCP.21.011059>].
- [18] N. Kawamura, M. Aoki, J. Doornbos, T. Mibe, Y. Miyake, F. Morimoto et al., *New concept for a large-acceptance general-purpose muon beamline*, *Progress of Theoretical and Experimental Physics* **2018** (2018) 113G01 [<https://academic.oup.com/ptep/article-pdf/2018/11/113G01/26732914/pty116.pdf>].
- [19] M. Tabata and H. Kawai, *Progress in development of silica aerogel for particle- and nuclear-physics experiments at J-PARC*, *JPS Conf. Proc.* **8** (2015) 022004 [[1410.2439](https://arxiv.org/abs/1410.2439)].
- [20] P. Bakule, G. Beer, D. Contreras, M. Esashi, Y. Fujiwara, Y. Fukao et al., *Measurement of muonium emission from silica aerogel*, *Progress of Theoretical and Experimental Physics* **2013** (2013) 103C01 [<https://academic.oup.com/ptep/article-pdf/2013/10/103C01/7570592/ptt080.pdf>].
- [21] *Transportation of ultra slow muon on u-line, mlf, j-parc*, in *Proceedings of the 14th International Conference on Muon Spin Rotation, Relaxation and Resonance (μ SR2017)* DOI [<https://journals.jps.jp/doi/pdf/10.7566/JPSCP.21.011060>].
- [22] M. Otani, N. Kawamura, T. Mibe, T. Yamazaki, K. Ishida and G. Marshall, *Tupak007: Progress on the muon g-2/edm experiment at j-parc*, in *Proceedings of the 9th International Particle Accelerator Conference (IPAC 2018)*, (Vancouver, Canada), p. TUPAK007, 2018.
- [23] Y. Kondo, K. Hasegawa, M. Otani, T. Mibe, M. Yoshida and R. Kitamura, *Beam dynamics design of the muon linac high-beta section*, *Journal of Physics: Conference Series* **874** (2017) 012054.
- [24] P. Strasser et al., *New muonium HFS measurements at J-PARC/MUSE*, *Hyperfine Interact.* **237** (2016) 124.
- [25] H. Iinuma, H. Nakayama, K. Oide, K. i. Sasaki, N. Saito, T. Mibe et al., *Current status of the muon g-2/edm experiment at j-parc*, *Nuclear Instruments and Methods in Physics Research Section A* **832** (2016) 51.
- [26] Y. Sato, M. Ikeno, T. KISHISHITA, T. Kohriki, T. Kume, T. Mibe et al., *Development of silicon strip detector for j-parc muon g-2/edm experiment*, p. 541, 08, 2019, DOI.
- [27] T. Bilka, N. Braun, T. Hauth, T. Kuhr, L. Lavezzi, F. Metzner et al., *Implementation of genfit2 as an experiment independent track-fitting framework*, *arXiv: Data Analysis, Statistics and Probability* (2019) .

- [28] C.D. Hendricks, *A study of the cyclotron*, Tech. Rep. UCRL-1234, U.S. Atomic Energy Commission (1959).
- [29] J. McCarthy, *Recursive functions of symbolic expressions and their computation by machine, part i*, *Commun. ACM* **3** (1960) 184–195.
- [30] R.O. Duda and P.E. Hart, *Use of the hough transformation to detect lines and curves in pictures*, *Commun. ACM* **15** (1972) 11–15.
- [31] NVIDIA Corporation, “CUDA C++ Programming Guide: GPU Memory Model.”
<https://docs.nvidia.com/cuda/cuda-c-programming-guide/index.html>.
- [32] NVIDIA Corporation, “NVIDIA Visual Profiler (nvprof).”
<https://docs.nvidia.com/cuda/profiler-users-guide/index.html>.
- [33] NVIDIA Corporation, “Nvidia tesla p100 gpu architecture.”
<https://images.nvidia.com/content/tesla/pdf/nvidia-tesla-p100-PCIe-datasheet.pdf>, 2016.
- [34] NVIDIA Corporation, “Nvidia rtx a6000 datasheet.”
<https://www.nvidia.com/content/dam/en-zz/Solutions/design-visualization/rtx/rtx-a6000/datasheet.pdf>, 2022.
- [35] NVIDIA Corporation, “Nvidia geforce rtx 4090 specifications.”
<https://www.nvidia.com/en-us/geforce/graphics-cards/40-series/rtx-4090/>, 2022.
- [36] NVIDIA Corporation, “Nvidia h200 tensor core gpu.”
<https://www.nvidia.com/en-us/data-center/h200/>, 2023.